Measurement of thermal conductivities of drill cuttings and quantification of the contribution of thermal conduction to the temperature log of the Hachimantai geothermal field, Japan

AUTHOR(S):

Sugamoto, Haruto; Ishitsuka, Kazuya; Lin, Weiren; Sakai, Takemi

CITATION:

Sugamoto, Haruto ...[et al]. Measurement of thermal conductivities of drill cuttings and quantification of the contribution of thermal conduction to the temperature log of the Hachimantai geothermal field, Japan. Geothermics 2023, 112: 102742.

ISSUE DATE:

2023-07

URL:

http://hdl.handle.net/2433/284029

Geothermics 112 (2023) 102742

Contents lists available at ScienceDirect

Geothermics

journal homepage: www.elsevier.com/locate/geothermics

Measurement of thermal conductivities of drill cuttings and quantification of the contribution of thermal conduction to the temperature log of the Hachimantai geothermal field, Japan

Haruto Sugamoto [a], Kazuya Ishitsuka [a,*], Weiren Lin [a], Takemi Sakai [b]

[a] Graduate School of Engineering, Kyoto University, Nishikyo-ku, Kyoto, Japan
[b] Geothermal Engineering Co., Ltd., Takizawa, Iwate, Japan

ARTICLE INFO

Keywords:
Drill cuttings
Thermal conductivity
Transient plane source method
Pyroclastic rock
Igneous rock
Temperature profile

ABSTRACT

This study proposed and evaluated a method of measuring the thermal conductivity (TC) of drill cuttings from several igneous and pyroclastic rocks using the transient plane source principle, which allows quick and reliable measurements. The estimated bulk TCs of rocks were within an error of <10%, and suitable models were found. Measurements were applied to drill cuttings obtained along a well in the Hachimantai geothermal field, Japan, and TCs were obtained at ~25 m intervals to a depth of 1700 m. Our analysis of the temperature profile using estimated TCs suggest the possible presence of fluid-flow zones in the well.

1. Introduction

Thermal conductivity (TC) is a vital physical property of rocks, particularly in geothermal studies. TC describes the amount of heat transfer via conduction in a medium per unit thermal gradient (Beardsmore and Cull, 2001) and has been used to quantify heat flow (Flovenz and Saemundsson, 1993; Pribnow and Sass, 1995; Zhang et al., 2018), delineate thermal properties in hydrothermal simulations (Hartmann et al., 2008), and characterize reservoirs and surrounding media (Li et al., 2020; Lippert et al., 2022). Furthermore, dense measurements of TCs along a well, combined with a temperature log, enable the identification of fluid-flow zones (Haffen et al., 2013). Thus, accurate and dense measurements of TCs are key to better understand heat transfer and underground fluid flow.

The TCs of rocks are generally obtained from measurements of rock cores (Pribnow and Sass, 1995; Popov et al., 1999). However, acquiring cores from deep locations and fractured reservoirs is expensive and difficult; thus, cores along most geothermal wells with high spatial densities have rarely been measured. Thermal response test (TRT) has been used to estimate effective TC in the ground, especially for the design of ground-coupled heat pump systems (Sanner et al., 2013; Zhang et al., 2014; Spitler and Gehlin, 2015). However, the applications of TRT are limited to shallow formations (300–500 m depth), and the estimated TCs by TRT are influenced by groundwater flow and the heterogeneity of surrounding formations (Zhang et al., 2014). In addition, active distributed temperature sensing using optical fibers has been applied to obtain the TC depth profile along a borehole (Maldaner et al., 2019). However, its applicable depth range is also shallow (less than 100 m) because of its complicated operation. Alternatively, drill cuttings are often obtained during geothermal energy investigations and exploration. The development of a method for measuring rock TC from drill cuttings or rock fragments has therefore been an important research topic (Sass et al., 1971; Morgan, 1975; Lee et al., 1986; Kiyohashi et al., 1991; Alonso-Sánchez et al., 2012; Rey-Ronco et al., 2013; Popov et al., 2018; Kämmlein and Stollhofen, 2019; Yi et al., 2021). Generally, TCs of cuttings are measured as the cuttings are immersed in water, and the TC of the solid (mineral part) and/or bulk (intact core equivalent) quantity is calculated using a physical formula (e.g., the mixing law).

Historically, steady-state methods have been proposed to measure TC of drill cuttings (e.g., divided-bar) (Sass et al., 1971; Morgan, 1975; Lee et al., 1986). Subsequently, transient measurement methods have recently been developed, mainly owing to the short measurement time, using the point source (Alonso-Sánchez et al., 2012; Rey-Ronco et al., 2013), optical scanning (Popov et al., 2018), line source (Kiyohashi et al., 1991; Kämmlein and Stollhofen, 2019), and plane source methods (Yi et al., 2021). Although these previous studies have shown the

Abbreviations: TC, thermal conductivity; QI, quartz index; XRD, X-ray powder diffraction; RD, relative difference; TRT, thermal response test.

* Corresponding author.
E-mail address: ishitsuka.kazuya.4w@kyoto-u.ac.jp (K. Ishitsuka).

https://doi.org/10.1016/j.geothermics.2023.102742
Received 2 February 2023; Received in revised form 10 April 2023; Accepted 27 April 2023
Available online 8 May 2023

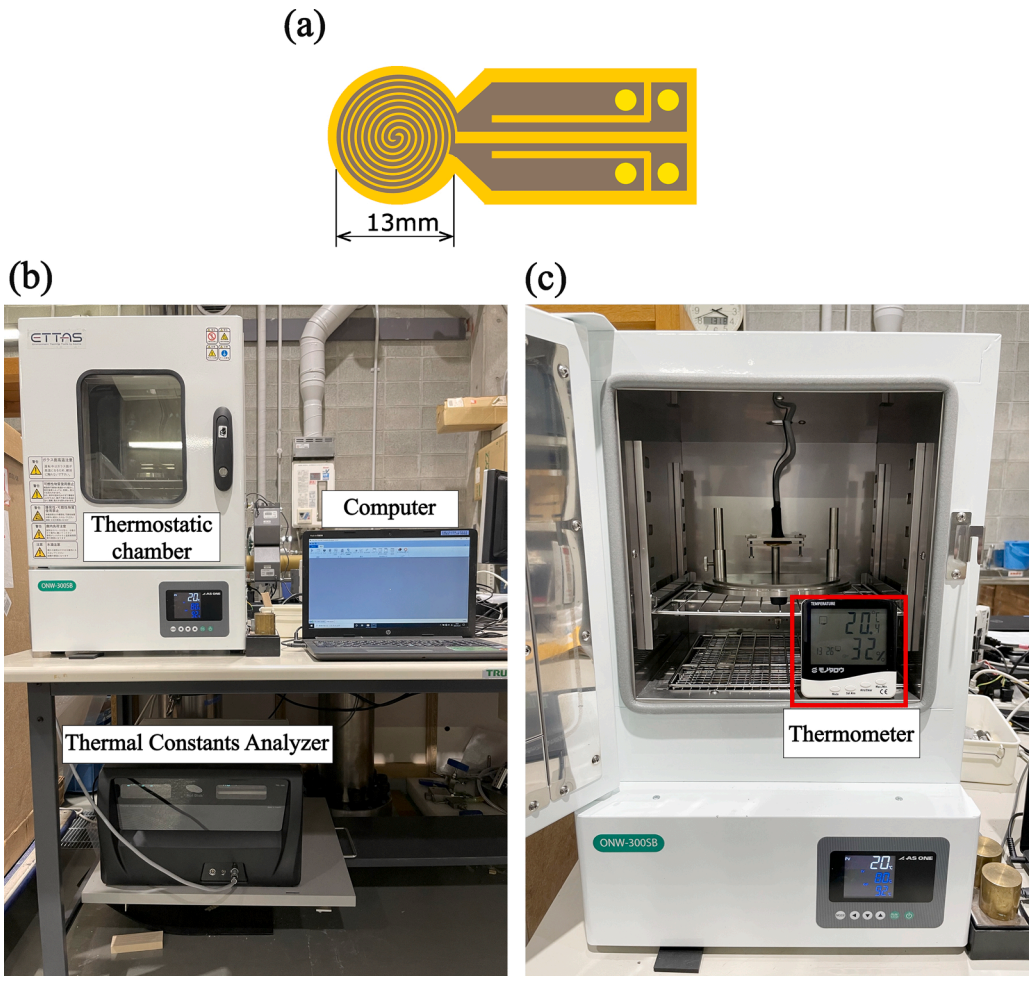

Fig. 1. The measurement instruments of the transient plane source method. (a) Schematic figure of the nickel helix sensor (Lin et al., 2014). (b) Measurement environment used in this study; thermal constants analyzer (Hot Disk TPS 1500) connected with computer to record measurement data. (c) The thermostatic chamber in which samples were measured to prevent significant changes in temperature and wind, and the thermometer used to check the room temperature before measurement.

effectiveness of these methods, some have been applied to only shallow depths (< 100 m) (Alonso-Sánchez et al., 2012) or sedimentary rocks (Kämmlein and Stollhofen, 2019). As volcanic regions are among the major play types for commercial geothermal energy operations (Moeck, 2014), and deep wells (> 1000 m) are generally drilled, the feasibility and impact of measuring TCs of drill cuttings along wells in geothermal operations remains unclear. Kiyohashi et al. (1991) showed the effectiveness of their method in measuring TC of drill cuttings at depths of 1500–1800 m in the Satsunan geothermal area, Japan, comprising tuff and dacite. However, a more recent method may improve the complexity and accuracy of these measurements, and its effectiveness in other species of igneous and pyroclastic rocks, which often occur in geothermal fields, must be investigated further.

Here, a new method for the measurement of solid and bulk TC from drill cuttings was proposed and examined by developing an original measurement probe based on the transient plane-source method. The transient plane source method has the advantage of a rapid and reliable measurement of TC and thermal diffusivity over a wide range of materials in a non-destructive way, owing to its design and the sensor's electrical resistance (He et al., 2005). Further, this method has been registered as a standard method to measure thermal properties by international organizations for standardization (ISO 22007–2, 2008). Moreover, compared to other transient methods, the proposed method requires a small cutting size (~50 g in this study) and a short measurement time (~10 min/measurement in this study) (Mathis, 2000). Taking advantage of the proposed method for fast and reliable TC determination, our modified method was applied to drill cuttings obtained along a borehole (to approximately 1700 m depth) in the Hachimantai geothermal field, within the Sengan area, which is one of the prominent geothermal fields in northeastern Japan (Akatsuka et al., 2022). The Matsuo-Hachimantai geothermal power plant started commercial production of 7.49 MW in this area in January 2019. Several Quaternary volcanoes are distributed, comprising the Hachimantai volcanic group, surround the geothermal area. Hot springs and hydrothermal alteration zones are distributed as surface manifestations of these geothermal activities (Akatsuka et al., 2022).

Drill cuttings were obtained, but rock cores were not retrieved from the target well. Therefore, to validate the proposed measurement method, cuttings were prepared by manually crushing rock cores from several volcanic areas in Japan, and the TCs from these cuttings and rock cores were compared. The effects of the particle size distribution of the drill cuttings and mixing models on the estimation performance were further assessed. The measured TC of drill cuttings does not directly express the bulk TC because the inter-particle spaces of drill cuttings are filled with water. Thus, it is important to determine a suitable mixing model that obtains solid and bulk TC from the measured TC of a drill cuttings and water mixture. Although the geometric model has been applied as a standard mixing model for the conversion of the measured TC from cuttings to solid and bulk TC (Sass et al., 1971; Lee et al., 1986; Kiyohashi et al., 1991; Lin et al., 2011; Alonso-Sánchez et al., 2012; Rey-Ronco et al., 2013; Popov et al., 2018; Kämmlein and Stollhofen, 2019; Lin et al., 2020; Yi et al., 2021), a suitable mixing model has not yet been fully developed. As discussed in recent studies on bulk TC estimation using rock core samples (Fuchs et al., 2013; Ray et al., 2015; Chopra et al., 2018; Fuchs et al., 2018), the selection of a mixing model is important to accurately determine bulk TC from cuttings. Moreover, the temperature log of the well was examined using the estimated bulk TCs. This analysis identified the heat flow and depth intervals at which

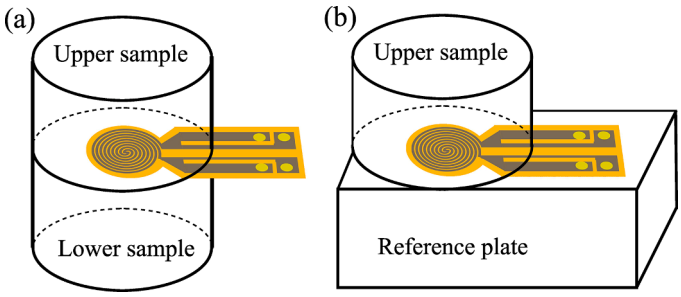

Fig. 2. Measurement modes of hot disk method: (a) Double-sided mode and (b) Single-sided mode. (Based on Lin et al., 2014).

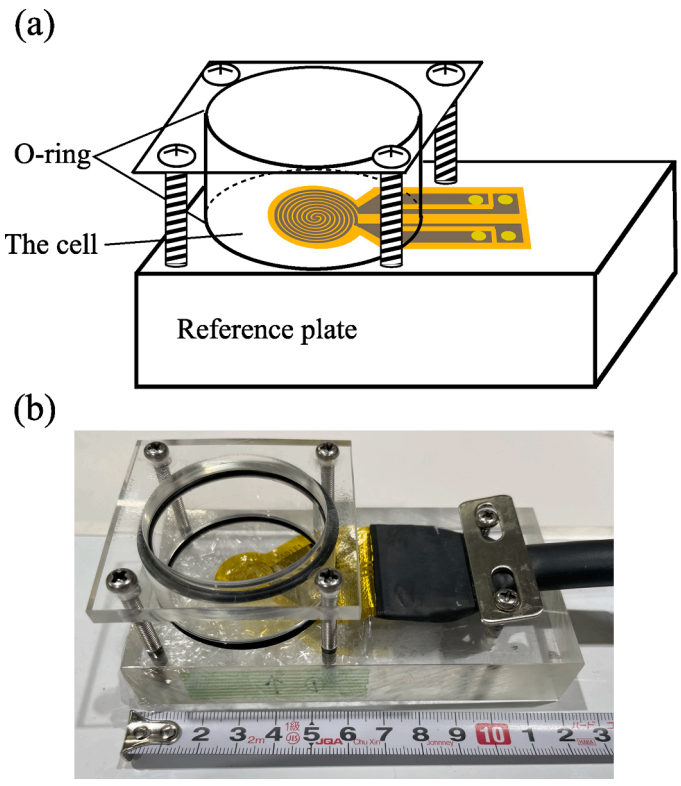

Fig. 3. A schematic figure of the probe for cutting measurements. (a) The cell is a hollow acryl cylinder with an inner diameter of 47.38 mm and outer diameter of 50.23 mm, filled with rock cuttings and water. The cell is pinned using two O-rings and four screws to prevent water from spilling out of the cell. The figure of the sensor is based on Lin et al. (2014). (b) A photograph of the probe.

temperature was affected by influences other than heat conduction (e.g., heat convection by fluid migration).

This study is the first to estimate the TCs of drill cuttings along a geothermal well and quantitatively evaluate the effect of the heat transfer pattern included in the temperature log. Additionally, this study examines the influences of selecting the mixing model and cutting particle size on the accuracy of measuring cutting TCs in volcanic areas. This study further showed that the quartz index (QI), which is relatively easy to obtain by X-ray powder diffraction (XRD) analyses, correlates with solid TC, and can therefore be used to understand the relationship between mineral components and solid TCs.

2. Methodology

2.1. Transient plane source method

The transient plane source method measures TC and thermal

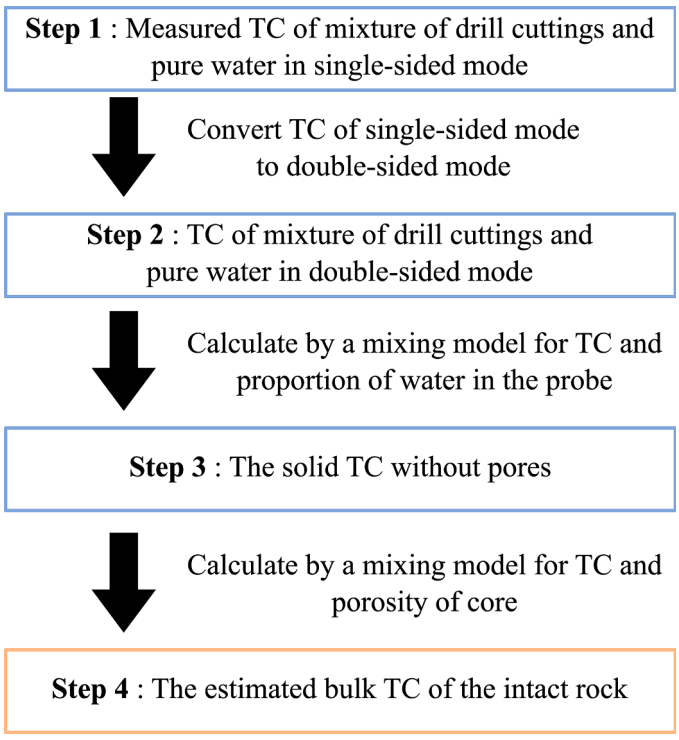

Fig. 4. Workflow to obtain the estimated bulk thermal conductivity (TC) of the intact rock from measured TC of cuttings.

diffusivity and was developed by Gustafsson (1991). A theoretical description of this method can also be found in He (2005). It is also referred to as the hot disk method and requires the use of a nickel helix sensor (Fig. 1a) and thermal constants analyzer (Fig. 1b).

The sensor functions as the heater and thermometer. It measures the changes in electrical resistance and records the temperature of the samples over time. Next, the TC of the sample is calculated from the temperature-time curve recorded by the thermal constants analyzer. In this study, the rock cutting samples and sensor were set in the thermostatic chamber and the TC was measured using a Hot Disk TPS 1500 Thermal Constants Analyzer (Fig. 1b and c).

The transient plane source method has two measurement modes: single- and double-sided (Fig. 2). In the double-sided mode, the sensor is between two samples, which can be either a solid or powder material, whereas the single-sided mode uses a sample on one side and a reference plate on the other. The reference place is thermally insulated to avoid the influence of thermal conduction from the reference plate; however, a sample with a certain thermal property can be acceptable as the reference plate. In this study, the TCs of core samples and drill cuttings were measured using the double-sided and single-sided modes, respectively. For TC measurements in the single-sided mode, an acryl plate was used as the reference (Fig. 3).

Fig. 3 shows the original measurement probe used to measure drill cuttings in the transient plane source method. The original probe has high durability for any measurement and is watertight for packing drill cuttings and water. As the TCs measured by single- and double-sided modes are not identical, the TCs measured in single-sided mode were corrected as described in Section 2.2.1 in more detail.

Yi et al. (2021) also used the transient plane source method for the TC measurement of drill cuttings, in which drill cuttings were ground to make fine powder under 75 μm, placed into an aluminum pan, and measured in double-sided mode. However, the present study proposed measuring drill cuttings in the single-sided mode without manual grinding for simplicity (Fig. 3).

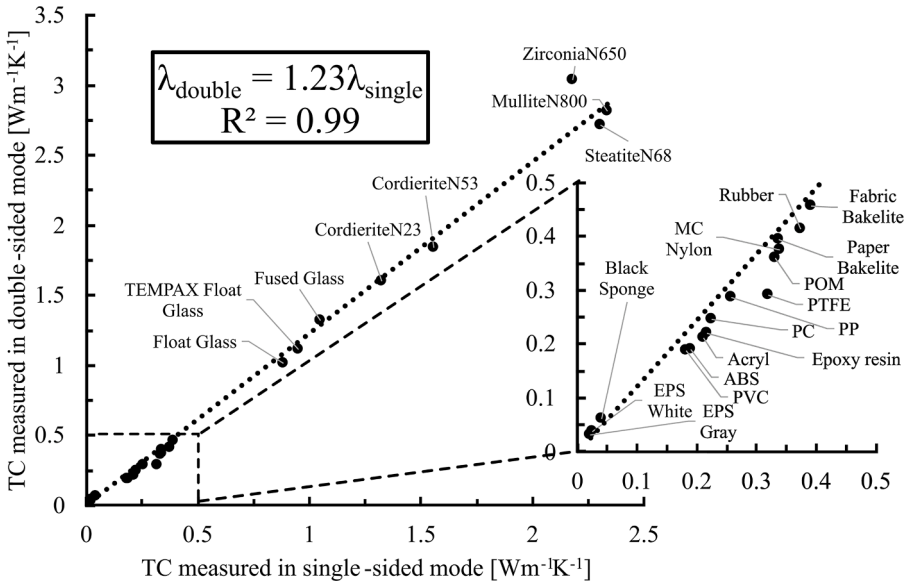

Fig. 5. Empirical calibration curve of the relationship between the thermal conductivity (TC) values measured in single- and double-sided modes, respectively. EPS: expanded polystyrene, PVC: polyvinyl chloride, ABS: acrylonitrile butadiene styrene, PC: polycarbonate, PP: polypropylene, PTFE: polytetrafluoroethylene, POM: polyacetal, MC Nylon: monomer casting nylon.

2.2. Calculation of bulk thermal conductivity from drill cuttings

2.2.1. Measurements and calculation

The measurement and calculation flow of bulk TC from the cuttings is shown in Fig. 4.

(Step 1) The TC of the mixture of drill cuttings and pure water was measured in the single-sided mode (Fig. 3). For this measurement, the drill cuttings were randomly packed in the probe and immersed in water. To avoid changes in environmental temperature and wind, measurements were conducted in a thermostatic chamber at 20–25 °C (Fig. 1b).

(Step 2) The measured TC value of the single-sided mode was converted into the TC value of the double-sided mode. This conversion required a reliable TC because the acryl used in the reference plate for the single-sided measurement is not a completely thermally insulated material. Thus, a calibration curve was created, which linked the thermal conductivities in the single- and double-sided modes using the measurements from 23 samples in both modes (Fig. 5), with steady and independent TCs, controlled temperature and humidity, and covering a wide range of rocks.

(Step 3) The solid TCs of the drill cuttings without the effect of water were estimated using the proportion of water in the probe and mixing models for TC. The proportion of water in the probe was obtained using the buoyancy method according to the following equation:

$$\phi_p = \frac{\frac{m_w}{\rho_w}}{\frac{m_w}{\rho_w} + \frac{m_c}{\rho_c}} \tag{1}$$

where ϕ_p is the proportion of water in the probe, m_w is the mass of water in the probe, m_c is the mass of cuttings in the probe, ρ_w is the density of water, and ρ_c is the particle density of cuttings. The TC of water (0.60–0.61 $Wm^{-1}K^{-1}$ at 20–25 °C) is calculated according to Sharqawy (2013) at room temperature in the chamber. The mixing models evaluated in this study are described in Section 2.2.2.

(Step 4) The bulk TC of the intact rock, which corresponds to the core-equivalent quantity, was calculated using a mixing model considering the solid TC and porosity of the core. The same mixing model as that used in Step 3 was applied. As discussed in the introduction, core samples were not available in the target well of the Hachimantai geothermal field. Thus, porosity measurements of the drill cuttings obtained from the target well were used instead of those from the core. To measure the mass of the wet drill cuttings for porosity calculations, we used the pycnometer method, in which drill cuttings were immersed in a vacuum for 30 min before the porosity of the cuttings was measured according to Kiyohashi et al. (1989).

2.2.2. Mixing models for thermal conductivity

The mixing models for TC consider bulk TC the result of the composite material of minerals (i.e., solids) and pore fluids (i.e., liquids) based on the proportion of each phase for a water-saturated rock. To determine a suitable mixing model to link core- and cutting-derived TCs, five candidate mixing models were used and examined for accuracy.

Arithmetic model (Voigt, 1928; Reuss, 1929):

$$\lambda_b = (1-\phi)\lambda_s + \phi\lambda_w \tag{2}$$

Harmonic model (Voigt, 1928; Reuss, 1929):

$$\lambda_b = \frac{1}{\frac{(1-\phi)}{\lambda_s} + \frac{\phi}{\lambda_w}} \tag{3}$$

Geometric model (Lichtenecker, 1924):

$$\lambda_b = \lambda_s^{1-\phi}\lambda_w^{\phi} \tag{4}$$

Square root model (Adler et al., 1973; Robertson and Peck, 1974):

$$\sqrt{\lambda_b} = (1-\phi)\sqrt{\lambda_s} + \phi\sqrt{\lambda_w} \tag{5}$$

Effective medium model (Bruggeman, 1935; Hanai, 1968; Sen et al., 1981; Clauser, 2009):

$$\lambda_b = \frac{1}{4}\left\{3\phi(\lambda_w-\lambda_s) + 2\lambda_s - \lambda_w + \sqrt{9\phi^2\lambda_s^2 + 18\phi\lambda_s\lambda_w - 18\phi^2\lambda_s\lambda_w - 12\phi\lambda_s^2 + \lambda_w^2 - 6\phi\lambda_w^2 + 4\lambda_s\lambda_w + 9\phi^2\lambda_w^2 + 4\lambda_s^2}\right\} \tag{6}$$

where λ_b is the bulk TC ($Wm^{-1}K^{-1}$), λ_s is the TC of the solid medium ($Wm^{-1}K^{-1}$), λ_w is the TC of water ($Wm^{-1}K^{-1}$), and ϕ is the volumetric fraction of water.

The arithmetic model (Eq. (2)) refers to the apparent bulk TC when the composition phases in the rock are arranged parallel to the direction of heat flow. This model may be suitable for situations such as igneous intrusion, tight folding, and salt-pluming (Beardsmore and Cull, 2001). The harmonic model (Eq. (3)) indicates the apparent bulk TC when the phases in the rock are layered perpendicular to the direction of heat flow. This model is suitable in conditions such as the alternation of sandstone and shale (Beardsmore and Cull, 2001). The geometric model (Eq. (4)) describes a mixture of different minerals in which phases are randomly oriented (Beardsmore and Cull, 2001). This model is the most popular for calculating the estimated bulk TC from rock cuttings (e.g., Sass et al., 1971; Yi et al., 2021); however, it does not have an established physical basis (Roy et al., 1989). The square root model (Eq. (5)) is applicable when several compositions are randomly oriented, as with the geometric model. It is based on the electrical conductivity and percolation theory, which describes the connectivity of pores (Adler et al., 1973; Robertson and Peck, 1974). Beardsmore and Cull (2001) recommend the square root model as a standard, unless there are sensible reasons for using other models. The effective medium model (Eq. (6)) represents a situation in which spherical components, such as particles and pores, are randomly distributed (Sen et al., 1981; Clauser, 2009). In validation, suitable mixing models were evaluated using the relative difference (RD in%) equation shown below:

$$RD = \frac{\lambda_{b,e} - \lambda_{b,m}}{\lambda_{b,m}} \times 100 \tag{7}$$

where $\lambda_{b,m}$ is the measured TC of core ($Wm^{-1}K^{-1}$) and $\lambda_{b,e}$ is the estimated bulk TC ($Wm^{-1}K^{-1}$).

2.3. Comparison of mineral compositions

The estimated solid TCs from the well in the Hachimantai geothermal field were compared with mineral compositions using XRD data to determine high impact mineral against the solid TC. The New Energy and Industrial Technology Development Organization (NEDO 2007, 2009) and Ojima et al. (2020) conducted XRD analyses of drill cuttings along a well. The QI of each mineral at each borehole depth were defined as follows (Hayashi, 1979; Takahashi et al., 2007; Ishitsuka et al., 2022):

$$QI = \frac{I_m}{I_{cq}} \times 100 \tag{8}$$

where I_m is the peak intensity of a mineral, and I_{cq} is the peak intensity of pure crystallized quartz.

As the peak intensity of the XRD value is influenced by the amount of minerals, the QI often reflects the relative amount of minerals. Nonetheless, the peak intensity is affected by the crystallinity and preferential growth of the crystal structure; thus, the QI of clay minerals tends to be lower than that of other minerals. This analysis used the QIs of 17 minerals at each depth: four clay (smectite, chlorite, sericite, and kaolinite), two zeolite (laumontite and wairakite), three silica (cristobalite, tridymite, and quartz), two silicate (plagioclase and epidote), two oxide (magnetite and rutile), one carbonate (calcite), one sulfide (pyrite), and two sulfate minerals (anhydrite and gypsum).

To understand the relative importance of each mineral on solid TC, linear regression analysis between QIs and solid TCs was conducted. Drill cuttings at 57 out of 65 depths taken from the Hachimantai geothermal field were used, as QI data was lacking at the remaining 8 depths. The following linear relationship between the estimated solid TCs and the QIs of the 17 minerals was considered, and the coefficients β_n and C were estimated by linear regression analysis:

$$\lambda_s = \sum_{n=1}^{17} \beta_n x_n + C \tag{9}$$

where λ_s is solid TC, β_n is the coefficient of each mineral, and x_n is the QI of the corresponding mineral. C is the constant. When the estimated coefficient of a mineral β_n has a larger value than that of other minerals, the mineral has a larger contribution to solid TCs. In the linear regression, we normalized the QI values to the maximum and minimum values of 1 and 0, respectively.

The linear regression was conducted by minimizing the objective function. To account for the effects of the objective function, the following two objective functions (S) were used: least square and lasso models.

Least square model:

$$S = \sum_{k=1}^{57} \left(\lambda_{s\_e,\ k} - \widehat{\lambda_{s,k}}\right)^2 \tag{10}$$

Lasso model:

$$S = \sum_{k=1}^{57} \left(\lambda_{s\_e,k} - \widehat{\lambda_{s,k}}\right)^2 + \alpha_l \sum_{n=1}^{17} |\beta_n| \tag{11}$$

where $\lambda_{s\_e,\ k}$ is the solid TC estimated by a mixing model at a depth of k, and $\widehat{\lambda_s}$ is the solid TC calculated by the linear regression. Constant α_l was set to 0.05. Generally, the estimated coefficient depends on the minimized objective function. The objective function of the least squares model is the sum of the squared residual $\sum_{k=1}^{57}(\lambda_{s\_e,k} - \widehat{\lambda_{s,k}})^2$, and evaluates the effects of all explanatory variables. The objective function of the lasso model contains the absolute value of the estimated coefficient $\sum_{n=1}^{17}|\beta_n|$ in addition to the squared residual. As the lasso model minimizes the magnitude of the coefficients, it tends to yield sparse estimates (i.e., most of the estimates are zero) compared to the least squares model.

2.4. Contributions of thermal conduction to the temperature log

After obtaining the bulk TCs from the drill cuttings along the well in the Hachimantai geothermal field, the heat flow and influence of thermal conduction on the temperature log were quantified according to the following three steps.

i) Assuming that heat is conducted in one direction along the well, the heat flux (Wm^{-2}) was calculated with a thermal gradient (Km^{-1}) and a harmonic average TC for a depth interval using Fourier's law (Eq. (12)) (Beardsmore and Cull, 2001):

$$q = -\lambda\ \mathrm{grad}T \tag{12}$$

where q is the heat flux (Wm^{-2}), λ is TC ($Wm^{-1}K^{-1}$), and grad$T$ is the temperature gradient (Km^{-1}).

ii) With reference to the temperature at the bottom of the depth interval, the temperature at the above depth interval was estimated based on the measured temperature and the bulk TCs of the depth interval (Eq. (13)). The calculation of the temperature was repeated at the shallowest depth.

$$T_{i-1} = T_i - \frac{q}{\lambda_i}(d_i - d_{i-1}) \tag{13}$$

where T_i is the temperature (°C) at a depth of i, q is the heat flux (Wm^{-2}), λ_i is the estimated bulk TC ($Wm^{-1}K^{-1}$) at a depth of i, and d_i is the depth (m) of i.

iii) The estimated and measured temperatures were compared to identify the temperature profile (thermal conduction or TC) at each depth interval. For a quantitative comparison, the absolute differences between the gradients of the measured and estimated temperature

Table 1
Rock sample list for the validation of the estimated thermal conductivity (TC) from cuttings.

Area (Japan)	Lithology	Sample ID	Depth [m]	Porosity of core [-]	Mean of measured bulk TC [$Wm^{-1}K^{-1}$]
Hachimantai	Andesite	HT-2	975.80–975.95	0.038	2.39
Kumamoto	Andesite	FDB-1-TP37	458.74–459.00	0.157	1.47
Kumamoto	Andesite	FDB-1-D2	472.00–472.42	0.126	1.39
Kumamoto	Tuffaceous conglomerate	FDB-1R-TP15	639.77–640.00	0.301	1.16
Kumamoto	Tuffaceous conglomerate	FDB-1R-D5	561.80–562.00	0.078	1.64
Awaji Island	Granite	NFD	932.36–932.60	0.025	2.88
Matsuyama	Granite	MAT	571.37–571.67	0.017	3.02
Hachimantai	Dacitic tuff	HT-9	779.05–779.20	0.203	2.20
Hachimantai	Dacitic tuff	HT-3	272.60–272.90	0.167	2.20

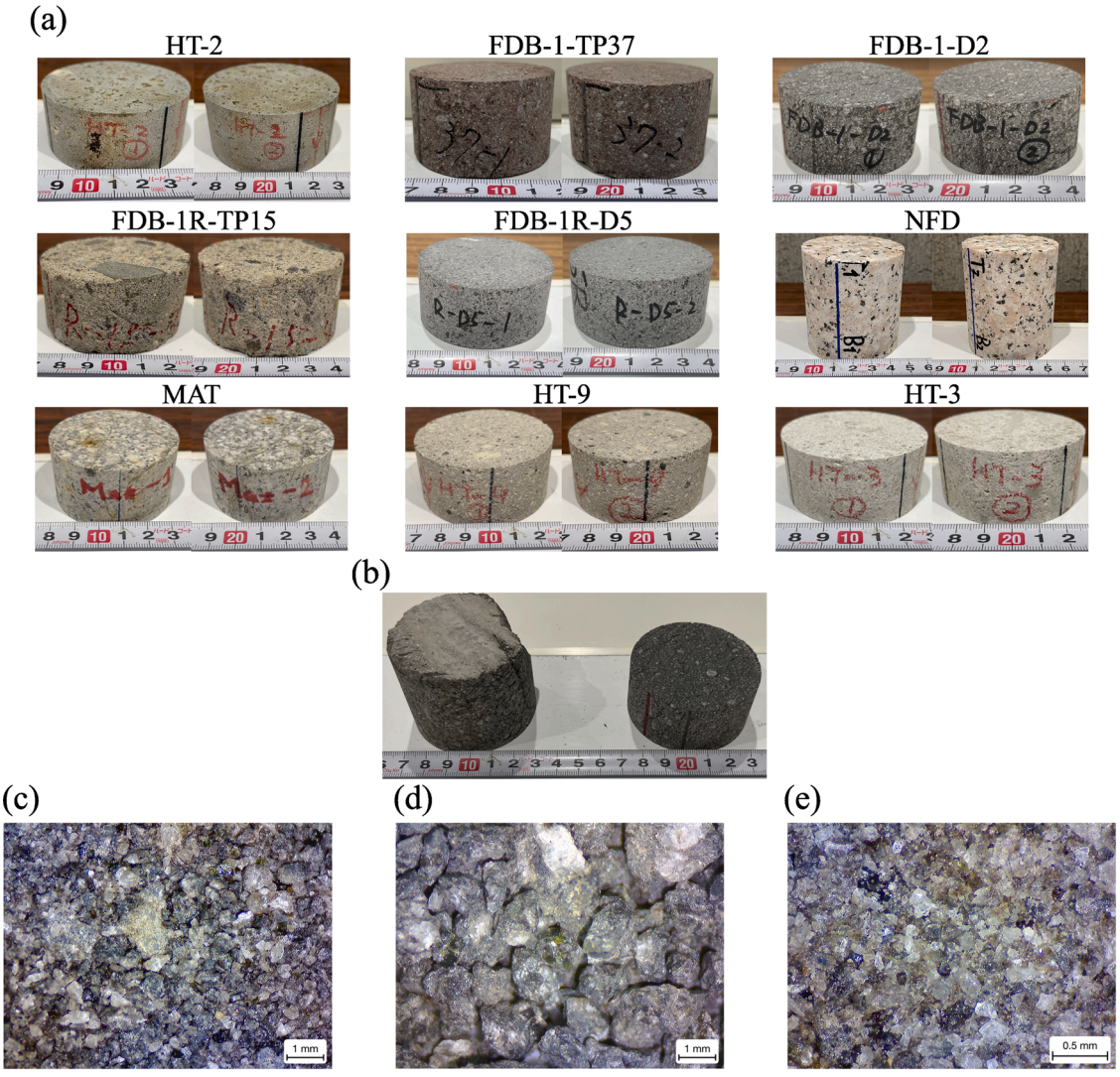

Fig. 6. Core samples and artificial cuttings. (a) Core samples for the validation of estimated bulk thermal conductivity. (b) Core samples of FDB-1-D2 for artificial cuttings and (c)-(e) artificial cuttings of FDB-1-D2. Particle sizes of (c) $d < 4$ mm, (d) 850 μm $\leq d <$ 4mm, (e) $d <$ 425 μm.

profiles at each depth were calculated. The absolute difference was calculated as follows:

$$Difference = |\mathrm{grad}T_{mea} - \mathrm{grat}T_{est}| \quad (14)$$

where $\mathrm{grad}T_{mea}$ and $\mathrm{grat}T_{est}$ are the gradients of the measured and estimated temperatures at each depth, respectively. $\mathrm{grad}_{mea}T$ is calculated by ± 12.5 m depths from a depth and the corresponding temperatures, and $\mathrm{grat}T_{est} = q/\lambda$ at the depth.

3. Rock samples and data

3.1. Rock samples for the validation of estimated bulk thermal conductivity

Nine core samples were used for validation, including three andesite cores (HT-2, FDB-1-TP37, and FDB-1-D2), two tuffaceous conglomerate cores (FDB-1R-TP15 and FDB-1R-D5), two granite cores (NFD and

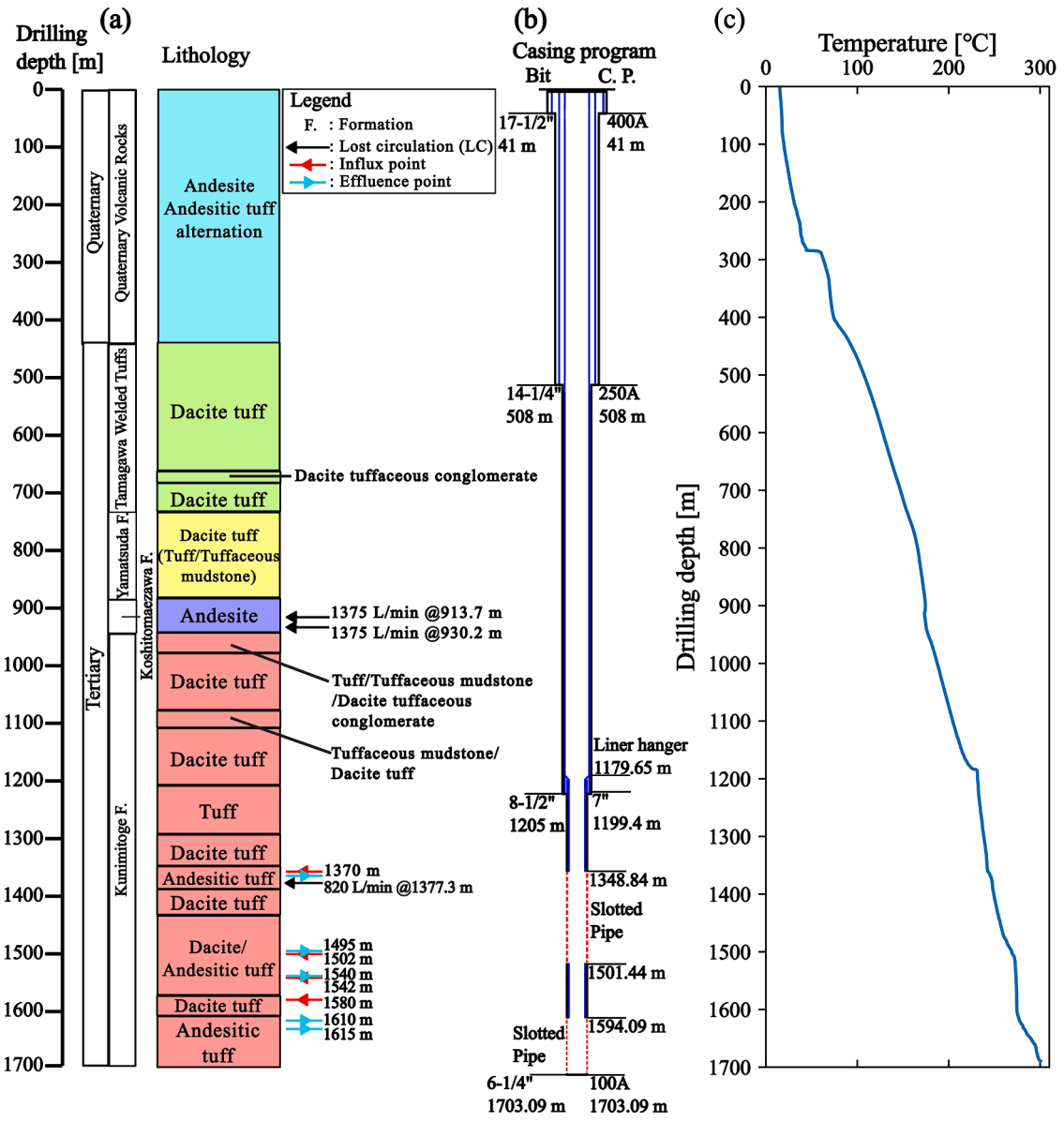

Fig. 7. (a) Lithology and potential flow point (lost circulation (LC), influx, and effluence point), (b) casing program, and (c) temperature profile measured on April 8, 2008 (139 d after circulation stopped) of the target well (modified from NEDO, 2009).

MAT), and two dacitic tuff cores (HT-9 and HT-3) (see Tables 1, S1 and Fig. 6).

The core samples with HT in their IDs were taken from other boreholes around the Hachimantai geothermal area. Those with IDs beginning with FDB were taken from the Aso volcanic area in the Kumamoto region of southwest Japan (Shibutani et al., 2022), and the cores with NFD and MAT IDs were taken from Awaji Island and the Matsuyama area, western Japan. The depths of these core samples and their measured porosities are listed in Table 1.

These core samples were cut into four subsamples; two subsamples were used to measure the TC of the core, whereas the other two were used to make the cuttings. The two subsamples for the cuttings were crushed manually and divided into three particle size distributions (particle size $d < 4$ mm, 850 μm $\leq d <$ 4 mm, and $d <$ 425 μm) to verify the effects of particle size on the accuracy of TC estimations. Fig. 6b shows an example of the FDB-1-D2 core samples used for making artificial cuttings, and its manually crushed cuttings of different particle size distributions are shown in Fig. 6c–e.

When the TCs were measured, the core samples had been immersed in pure water for 48 h in a vacuum for saturation, and the core samples for dry conditions had been put in an oven at 105 °C for 48 h. Cuttings were dried in an oven at 80 °C for 24 h. Dry samples were placed into the probe with pure water, and a weight of 438 g was placed on the cuttings in the probe to ensure their packing. TC was then measured in the single-sided mode six times (Fig. 3). After the measurement was completed, the artificial cuttings were dried, and the measurements were repeated three times for each particle size distribution and each sample.

3.2. *Drill cuttings and temperature log at the Hachimantai geothermal field*

The Hachimantai geothermal field is located in northeastern Japan and is part of the Hachimantai volcanic group (Akatsuka et al., 2022). Acid alteration comprising silicified alteration, alunite, pyrophyllite, and kaolin minerals are found on the surface of the field (NEDO, 2007).

The drilling depth of the target well was 1703 m (Fig. 7). Similar to the surrounding geology, Quaternary tuff and lava are overlaid on Tertiary dacitic and andesitic tuffs (Fig. 7a) (Kimbara, 1985).

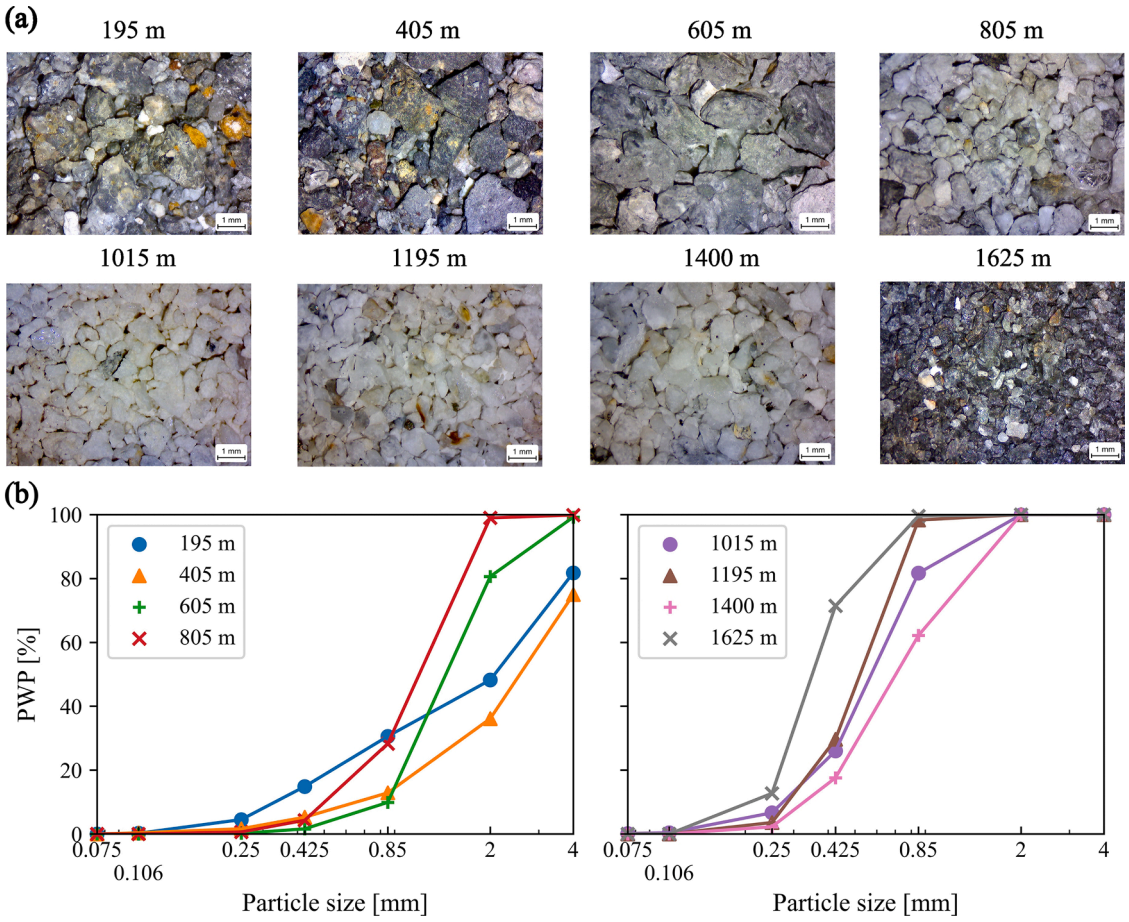

Fig. 8. Examples of drill cuttings obtained in the well (depth spacing about 200 m). (a) Microphotographs of the drill cuttings, and (b) particle size distribution of the drill cuttings shown in (a). PWP: Passing weight percent.

Quaternary tonalite intrudes beneath the Tertiary formation, and XRD analyses identified the extensive development of metamorphic minerals (e.g., biotite, cordierite, magnetite, and orthopyroxene) at the margin of the Tertiary groups and Quaternary intrusive bodies at depths of > ~1500 m (NEDO, 2007, 2009). The XRD analyses further identified a clay alteration zone comprising smectite below ~500 m, which may have functioned as a caprock layer (NEDO, 2007, 2009). The minerals formed by hydrothermal alteration along the target well was classified by Ishitsuka et al. (2022). Fig 7a shows potential flow zones including lost circulation points and influx/effluence points (NEDO, 2009).

Fig. 7c shows the temperature log in the well (NEDO, 2009), which was measured approximately 6 months after the completion of drilling, i.e., after the temperature recovered from disturbances induced by drilling and mud circulation. Temperature gradually increases with depth and was about 300 °C at a depth of 1700 m, leading to an average temperature gradient of about 0.16 °C/m. Sudden changes in temperature are also found at several depth intervals: the temperature fluctuated around 285 m, corresponding with groundwater levels, and a sharp change in the temperature profile around 1179 m may have been due to the joint of casing and liner pipes (Fig. 7b and c) (NEDO, 2009). Pressure-Temperature-Spinner logging measured the downward heat convection in the well at approximately 1179 m depth (NEDO, 2009). NEDO (2009) reported that water moved up in an annulus between a 6.25 inch well and a 100A (outer diameter = 4.5 inch) liner pipe, entered the gap of the liner hanger, and moved down in the well. Considering these artificial effects on temperature logs, the log was divided into two depth intervals (305–1165 m and 1195–1675 m) and the contribution of thermal conduction to the temperature log was quantified at each depth interval, as described in Section 2.3.

Drill cuttings were obtained every 5 m along the well depth (NEDO, 2009). A total of 65 drill cuttings from 35 to 1700 m depth were measured at an interval of approximately 25 m. Fig. 8a shows examples of drill cuttings. Drill cuttings at depths of 195 and 405 m comprise andesitic and andesitic lapillus tuffs, respectively. Drill cuttings with dark colors contain a few sulfurs (Fig. 8a). The lithology of drill cuttings at 1015, 1195, and 1400 m depth with light colors comprise a dacitic tuff (Fig. 8a). Drill cuttings with dark colors at deep depths (e.g., > 1625 m) underwent thermal metamorphism (Fig. 8a). Particle size distributions showed that drill cuttings at depths of 195, 405, and 605 m have particle sizes of 2–4 mm (Fig. 8b). In the drill cuttings at a depth of 805–1400 m, particle size distribution showed a larger percentage of smaller particle sizes of 250–850 μm, but rarely particle sizes > 2 mm (Fig. 8b). Cuttings with particle sizes < 250 μm were found at a depth of 1625 m. Generally, the particle sizes become smaller when the depth of drill cutting is deeper (Fig. 8b).

4. Results

4.1. Validation of the estimated bulk thermal conductivities

Fig. 9 summarizes the results of RD values (Eq. (7)) between the measured bulk TC of the rock cores and the estimated bulk TCs of the artificial rock cuttings. Table 2 shows the average of the absolute RD values of the nine rock samples for each mixing model and particle size distribution. Detailed results of the estimated bulk TCs and RD values and the measurement data are shown in Tables S1–S4. For most of the samples, the evaluation of the mixing models showed that the RD values of the square root model were the smallest or the second smallest among

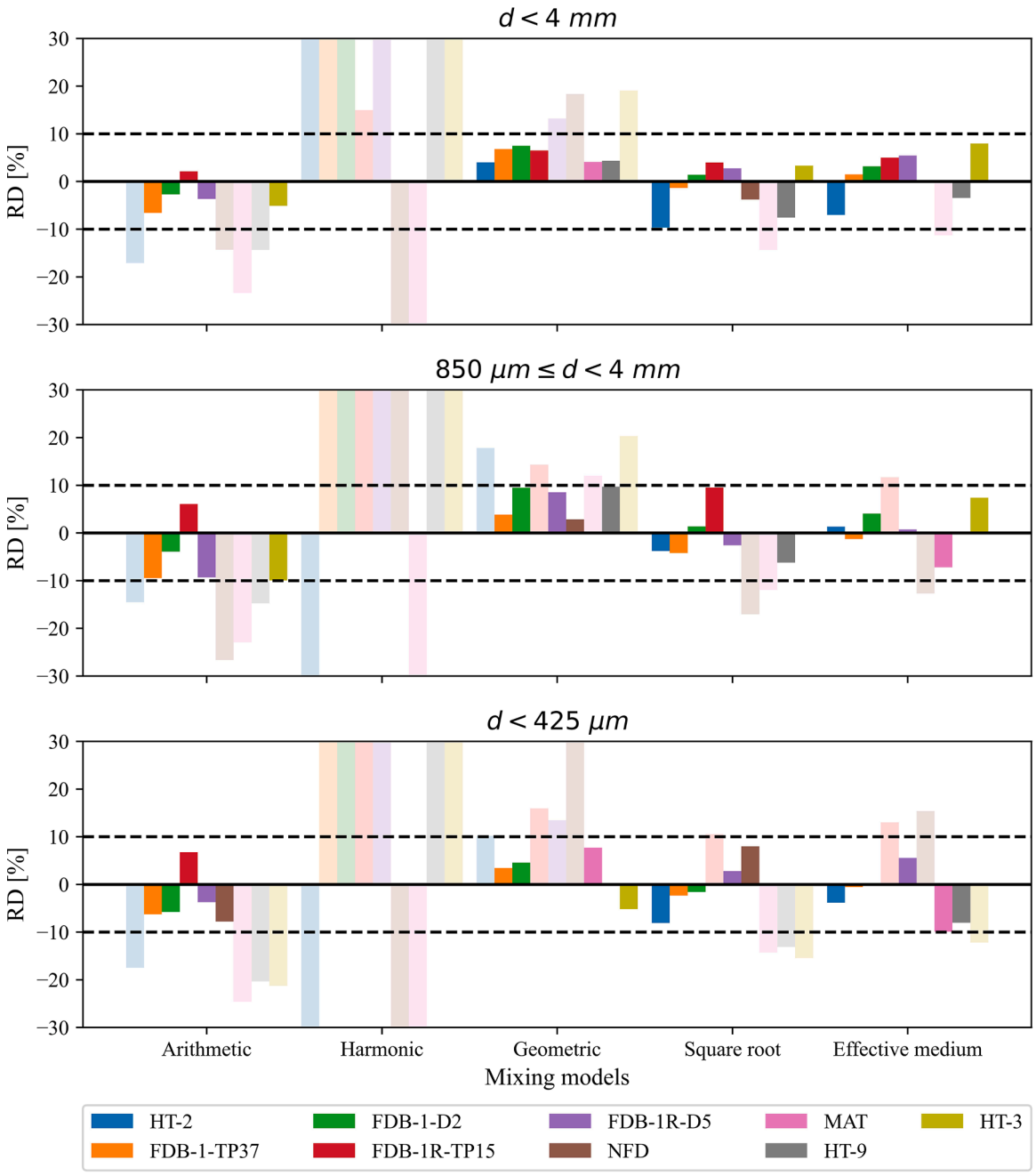

Fig. 9. The relative difference (RD) values (Eq. (7)) of each model, sample, and particle size distribution (d). Bars with RD values exceeding ±10% are drawn semi-transparently. In the legends, rock IDs shown in Table 1 are used. Detailed RD values are shown in Table S1.

the five mixing models examined in this study (Fig. 9). Most of RDs using the square root model were within ±5%, with a minimum of 1.4% for FDB-1-D2 (Fig. 9). The effective medium model also produced small RD values (−5% < RD < 5%), for example, in FDB-1-TP37, NFD, FDB-1-D2, HT-9, and RD values < 10% were observed in most of other rock samples (Fig. 9). Considering that most previous TC studies regarded absolute RDs < 10%–15% as a threshold for small errors (Sass et al., 1971; Kiyohashi et al., 1991; Fuchs et al., 2015), the estimated bulk TCs were sufficiently accurate. In addition, although RD values obtained from the arithmetic and geometric model tended to be negative and positive values, respectively, those from the square root and effective medium models had both positive and negative values, indicating that the calculated TCs from the latter models were less biased (Fig. 9).

The exceptions were MAT (granite), where the square root and effective mean models yielded large absolute RDs (~ 15%), suggesting the geometric model was the most suitable (Fig. 9). Although the geometric model was the most suitable for a few samples, our results showed that this mixing model often yielded large RD values (> 10%), for example, in FDB-1R-D5 and HT-3 (Fig. 9). On the other hand, the harmonic model yielded the worst RD values of > 100% or < −100% in most rock samples. Considering the average RD value of each model for all particle size distributions (right column in Table 2), the mean RD value of the effective medium model was the smallest, followed by the square root model. However, the difference between the mean values of the two models was minor. Thus, the square root and effective medium models are equally suitable for TC measurements of drill cuttings (Fig. 9).

To check whether the packing of drill cuttings was sufficient, different weight settings were imposed on the measurement probe filled with cuttings of FDB-1-D2: (i) weight of 438 g (the reference used in this

Table 2
Mean absolute RD values of each model and particle size distribution (d). Cell values show the average RD values of nine rock samples for each model and particle size distribution. $\overline{RD_m}$ is the mean RD value of all particle size distribution for each model, and $\overline{RD_{psd}}$ is the mean RD value of four mixing models (except for harmonic model) for each particle size distribution.

Particle size distribution Model	$d < 4$ mm	850 μm $\leq d < 4$ mm	$d < 425$ μm	$\overline{RD_m}$
Arithmetic	9.93 (±7.14)	13.07 (±7.12)	12.67 (±7.65)	11.89 (±7.44)
Harmonic	394.88 (±456.89)	355.81 (±318.53)	194.82 (±161.40)	315.17 (±345.81)
Geometric	9.30 (±5.67)	10.98 (±5.50)	11.83 (±12.90)	10.70 (±8.80)
Square root	5.36 (±4.11)	6.34 (±5.19)	8.47 (±5.01)	6.72 (±4.97)
Effective medium	5.01 (±3.22)	5.15 (±4.54)	7.65 (±5.14)	5.94 (±4.54)
$\overline{RD_{psd}}$	7.40 (±5.71)	8.89 (±6.54)	10.16 (±8.58)	

study), and (ii) weight of 875 g. The measured TCs of the single-sided mode (Step 1 in Fig. 4), before the conversion to solid and bulk TCs, were 0.891 $Wm^{-1}K^{-1}$ in setting (i) and 0.878 $Wm^{-1}K^{-1}$ in (ii). The measured TCs with weights of 438 and 875 g were almost identical (difference of ~1.4%). Thus, the influence of the weight put on the measurement probe is not significantly enhanced as the weight increases.

The comparison of the RD values from the different particle size distributions showed that the influence of particle size depended on lithologies. For the andesite samples (FDB-1-TP37, FDB-1-D2, and HT-2), the particle size did not significantly influence the estimated TCs (Fig. 9). However, particle size was relatively significant in granite (NFD, MAT) and tuffaceous conglomerate samples (FDB-1R-TP15, FDB-1R-D5), but the differences in RD values for each particle size distribution was only approximately 10% (Fig. 9).

Table 2 shows that the smallest mean was < 4 mm of the three distributions, and they did not significantly differ. The test of significance (Bulmer, 1979) was conducted to determine if the mean of the RD values obtained from different particle size distributions ($d < 4$ mm, 850 μm $\leq d < 425$ μm and $d < 425$ μm) were statistically different. Assuming that the RD values follow normal distribution and equal variances, analysis of variance (often referred to as ANOVA) was applied to the RD values to explore the null hypothesis that the averages of the RD values were statistically the same. The p-value of the test was 0.992 and much greater than the statistical significance level of 0.05 (5%); thus, the null hypothesis that the RD values obtained from the different particle size distributions are statistically same was not rejected. Consequently, the influence of the particle size distribution is less significant, and drill cuttings with an arbitrary particle size distribution of < 4 mm could be used. Considering these results, both the square root and effective medium models and drill cuttings with particle sizes < 4 mm were used to measure the TC of drill cuttings obtained in the Hachimantai geothermal area.

4.2. Estimated bulk thermal conductivity from drill cuttings

The TCs of the drill cuttings with particle sizes < 4 mm obtained in the Hachimantai geothermal field were measured, and the solid and bulk TCs at each depth based on the square root and effective medium mixing models were estimated (Fig. 10). The solid TCs were between 1.53 and 4.16 $Wm^{-1}K^{-1}$ (square root model) and 1.57 and 4.63 $Wm^{-1}K^{-1}$ (effective medium model) (Fig. 10). The effective medium model yielded slightly larger solid TCs than the square root model. Drill cuttings of each depth were measured in triplicate, as the same drill cuttings were repacked in each measurement after drill cuttings were dried. The standard deviation of the three measurements was 0.002–0.110 $Wm^{-1}K^{-1}$. The variation (uncertainties) of the measured TCs may be caused by how cuttings were packed into the probe, which may influence the variation of the estimated solid and bulk TCs as well. The porosity of the drill cuttings used for the estimation of bulk TC is also shown in Fig. 10. Regarding the cuttings at 1600 m depth, the porosity was not measured because the amount of obtained 0.85–4 mm cuttings were not sufficient. Thus, the porosity of the cuttings at 1600 m was estimated from the average porosity from 1575 m and 1625 m. Almost all drill cuttings had porosities of 0.04 to 0.29, except for drill cuttings at 925 m. Drill cuttings at 925 m showed a porosity of approximately 0.47, which was high considering the burial depth and its lithology (andesite). However, this high porosity may be reasonable because the depth interval of 913–930 m was reported as a lost circulation zone (Fig. 7) (NEDO, 2009). Owing to its high porosity, the bulk TC at 925 m was smaller than that at nearby depths. The measurement data from the 65 drill cuttings are shown in Table S5.

4.3. Mineral compositions and solid thermal conductivities of the well

Fig. 11 shows the estimated coefficients of the linear regression analysis. The estimated coefficients of both mixing models showed similar trends. Both models showed that the coefficient of quartz had the largest positive value among all the minerals. In addition, the least square regression revealed that the magnitudes of the estimated coefficients for smectite and rutile were larger than those of the other minerals, and the coefficients of other minerals were within ± 0.5.

4.4. Quantifying the contribution of thermal conduction

Temperatures along the target well were calculated based on the bulk TCs estimated by either the square root or effective medium model, and the differences between the estimated and measured temperatures were obtained (Fig. 12). The temperatures estimated by the square root and effective models were almost identical (Fig. 12a). The difference between the estimated temperatures derived from both models was 0.0–0.91 °C (Fig. 12a). The resulting heat fluxes of the interval from 305 to 1165 m using the square root and effective medium models were 353 Wm^{-2} and 371 mWm^{-2}, and 348 mWm^{-2} and 374 mWm^{-2} at the depth interval of 1195–1675 m (Table 3). Although the analyzed depth was divided into two intervals, the estimated heat fluxes of both intervals were similar.

The root mean squared error between the measured and estimated temperatures at 55 depths was 7.34 °C. At most depth intervals, the measured and estimated temperatures were generally consistent with each other, indicating that the general temperature pattern could be explained by thermal conduction (Fig 12). However, the largest difference in the temperature gradient in the interval of 305–1165 m was 0.18 °C/m (square root model) and 0.19 °C/m (effective medium model) at a depth of 925 m, and that within the interval of 1195–1675 m was 0.33 °C/m (square root model and effective medium model) at a depth of 1650 m (Fig. 12). The high porosity at a depth of 925 m (Fig. 10) may explain the large difference at this depth.

5. Discussion

5.1. Suitable mixing models

Despite the historical use of the geometric model to convert measured TC from cuttings to bulk TC, the results highlight that the geometric model was not suitable for TC estimation using drill cuttings.

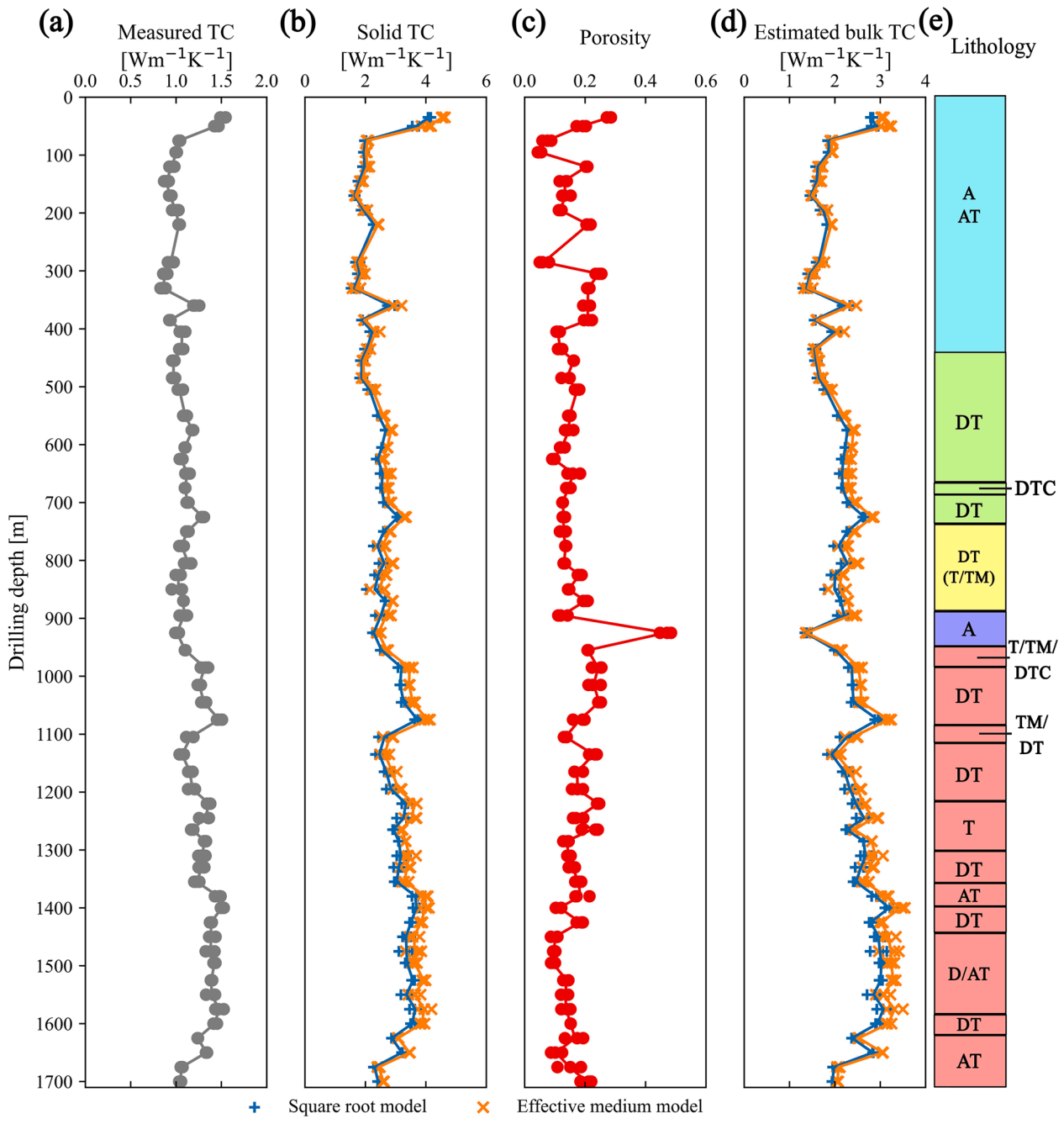

Fig. 10. (a) Measured thermal conductivities (TC) of a mixture of pure water and drill cuttings, (b) estimated matrix conductivities, (c) measured porosities and (d) bulk TCs at the target well. (d) Lithology of the well (same as in Fig. 7a). A, andesite; AT, andesitic tuff; DT, dacite tuff; DTC, dacite tuffaceous conglomerate; TM, tuffaceous mudstone.

The square root and effective medium models were found to be the most suitable among the five mixing models examined in this study, whereas the harmonic mean model was the least suitable. The following list ranks the mixing models examined in this study in the order of the mean error of the estimated TCs (Table 2).

Estimated Bulk TC Error : $\lambda er_{EM} \approx \lambda er_{SR} < \lambda er_{G} < \lambda er_{A} < \lambda er_{HM}$

where λer_{SR}, λer_{EM}, λer_{EM}, λer_{G}, λer_{A}, λer_{HM} are the errors in the estimated bulk TC derived using the square root, effective medium, geometric, arithmetic, and harmonic mean models, respectively.

As described in Section 2.2.2, the effective medium model assumes that spheres of mineral aggregates are oriented randomly, whereas the square root model is based on the percolation theory and conceptualizes a highly interconnected state between particles. These mixing models were speculated to yield the most accurate bulk TCs because these underlying assumptions are suitable for the randomly packed cuttings in the probe. The harmonic model yielded the worst estimation of bulk TCs in this study. Although this mixing model has been demonstrated to be the best for estimating solid TCs in low-porosity igneous and plutonic rock cores (Ray et al., 2015; Chopra et al., 2018; Fuchs et al., 2018), it may not be suitable for estimating TCs from random packings of cutting particles in the probe. The negative estimated bulk TCs from the harmonic model resulted in RD values > 100% (Table S1). Considering that Fuchs et al. (2013) reported that high porosity contributed to a negative value when calculating the bulk TC using the harmonic model, a high proportion of water in the probe (~0.5) may cause RD values > 100%.

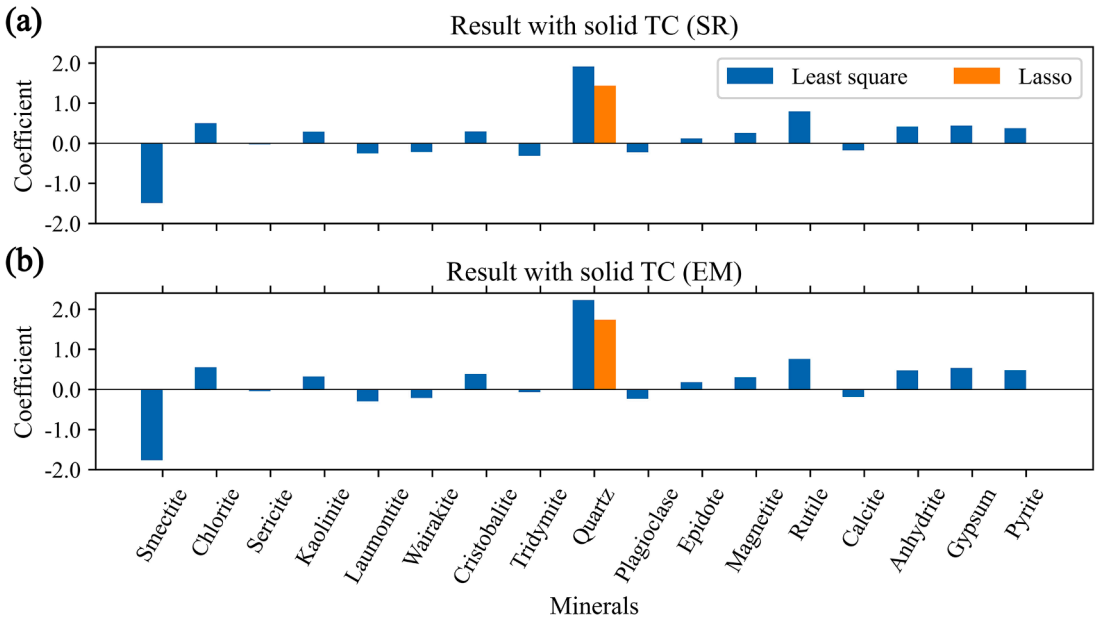

Fig. 11. The estimated coefficient of each mineral in Eq (9), which indicate the importance of each mineral to the estimated solid TC, by the linear regression analysis. (a) the estimated coefficients calculated from the matrix TC with square root (SR) model, and (b) those from the matrix TC estimated with effective medium (EM) model.

The errors in estimated TCs from the arithmetic model were small (RD < 10%) in some rock samples (e.g., FDB-1-TP37, FDB-1R-TP15, and FDB-1R-D5) (Fig. 9); however, this simple model yielded a large error (RD > 15%) in other samples. The arithmetic model also assumes an extraordinary layered pattern parallel to the direction of heat transfer (Beardsmore and Cull, 2001), which does not match all rock samples in this study. The geometric model, which has been widely used for bulk and solid TC estimation from cuttings, yielded small errors (RD < 10%) in most of rock samples used in this study (e.g., MAT, HT-2, HT-9). However, our results showed that this model sometimes yielded some large errors (e.g., NFD and HT-3). The results of this study did not provide consistent characteristics of rock types or structural properties (e.g., porosity) to which this geometric model could successfully be applied. The lack of a physical background for this model also hinders unified understanding. Although Fuchs et al. (2013) showed that the geometric model is optimal for estimating solid TCs from isotropic to weakly anisotropic sedimentary rock cores, elucidating the conditions under which the geometric model can be applied would be a topic of future research.

5.2. Impact of each mineral on the solid thermal conductivity of the well

The magnitude of the estimated coefficients of quartz, smectite, and rutile were larger than other minerals (Fig. 11). These minerals with a relatively large coefficients influenced the solid TCs. The characteristic pattern of QI matched the depth pattern of the solid TC, and the negative coefficient of smectite indicated that the solid TC decreased as the QI of smectite increased (Figs. 10 and 13). The TCs of alpha-quartz and rutile have been reported as 7.7 $Wm^{-1}K^{-1}$ and 5.18 $Wm^{-1}K^{-1}$, respectively (Brigaud et al., 1989, 1992; Harada et al., 2010), whereas smectite has a small TC of 1.9 $Wm^{-1}K^{-1}$ (Brigaud et al., 1989, 1992). Thus, the inclusion of quartz and rutile could increase the solid TC, whereas smectite could result in a decrease in the solid TC. As the coefficients of other minerals were within ± 0.5, these minerals had relatively small effects on solid TC.

5.3. Effects of fluid migration on temperature profile

The biggest difference in the gradient was found at a depth of 1650 m; in comparison, the temperature structure around 1500–1650 m depth was convex downward compared with the estimated temperature structure assuming pure thermal conduction (Fig. 12), suggesting that the heat convection influenced the temperature structure. NEDO (2009) reported the influx point at a depth of 1502 m and the effluence point at a depth of 1615 m (Fig. 7a). Thus, formation water possibly enters the well from the slot of the liner pipe over 1501 m and from the slot of the well around 1650 m (Fig. 7). The downward flow of water in a well, which comes from the upper to the lower lost circulation layer, contributes to the downward convex structure of the temperature profile (The Geothermal Research Society of Japan (GRSJ), 2014). Therefore, a down-cross flow in the well may exist at 1500–1650 m owing to influx/effluence points. The existence of this flow may also influence relatively high measured gradients at depths of 1495 and 1625 m, where difference values are also high (Fig. 7b). In addition to the temperature at depths of 1500–1650 m, Fig. 11c shows a large difference of ~0.18 °C/m at a depth of 925 m. As the LC points were reported at depths of 913.7 and 930.2 m (Fig. 7a), this may influence the temperature structure at these depths.

5.4. Error sources in thermal conductivity measurements

The errors of the estimated solid TCs were considered to originate mainly from two error sources: the random packing of drill cuttings and the measurement error of the transient plane source method. The mean and the standard deviation of the maximum difference between respective and the mean solid TC were 3.3±2.4% (square root model) and 3.6±2.6% (effective medium model) for 65 drill cuttings in the Hachimantai geothermal field measured 3 times at each depth, reflecting the error of the estimated solid TC. The errors of the estimated bulk TCs were also quantified from the cuttings at the Hachimantai field, and the mean and standard deviation of the maximum difference between respective and the mean bulk TC were 3.0±2.2% (square root model) and 3.3±2.4% (effective medium model). These errors of the bulk TCs were attributed mainly to both the solid TC error and the error of the measured porosities. To obtain more theoretical error of the bulk TC, the RDs of the bulk TC $\Delta\lambda_b$ of the mixing models were derived from the error of the solid TC $\Delta\lambda_s$ described above and the measured error of porosity $\Delta\phi$ based on the error propagation theory ($\Delta\lambda_b$ =

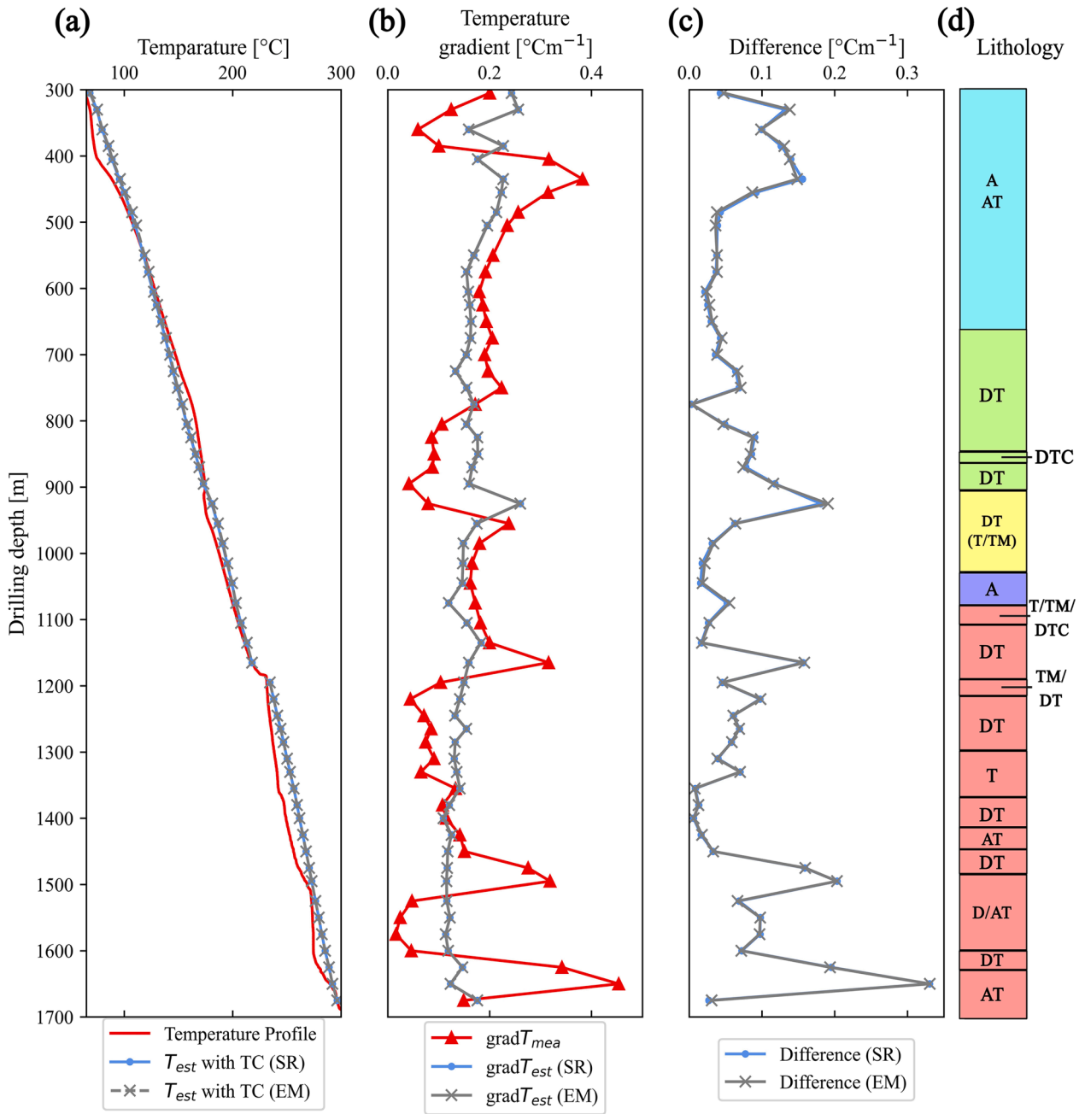

Fig. 12. (a) The measured and calculated temperature (T_{est}) of the target well. The blue line shows the estimated temperature using thermal conductivities (TCs) calculated using the square root (SR) model and the gray line shows TCs calculated with effective medium (EM) model. The red line indicates the temperature log. (b) The measured (gradT_{mea}) and estimated (gradT_{est}) temperature gradient at each depth. (c) The difference values from Eq. (14), which represent the difference between the gradients of estimated and measured temperatures. (e) Lithology of the well (Fig. 7). A, andesite; AT, andesitic tuff; DT, dacite tuff; DTC, dacite tuffaceous conglomerate; TM, tuffaceous mudstone.

Table 3
The estimated heat flux, respective measured temperature gradient (gradT_{mea}), and harmonic average of thermal conductivity (TC). SR and EM denote the square root and effective medium models, respectively.

Depth interval	Number of data	Estimated heat flux [mWm^{-2}]		Average of gradT_{mea} [°C/m]	Harmonic average of TC [Wm^{-1}K^{-1}]	
		SR	EM		SR	EM
305–1165 m	33	353	371	0.18 (±0.08)	2.00 (±0.36)	2.10 (±0.41)
1195–1700 m	22	348	374	0.13 (±0.11)	2.63 (±0.34)	2.82 (±0.38)

$\sqrt{(\Delta\lambda_s \cdot \partial\lambda_b/\partial\lambda_s)^2 + (\Delta\phi \cdot \partial\lambda_b/\partial\phi)^2}$). The measured error of porosity $\Delta\phi$ was also obtained as the maximum difference between respective and the mean porosities from each depth sample (measured 3 times) of 65 drill cuttings in the Hachimantai geothermal field. The error propagation analysis indicated that $\Delta\lambda_b$ were 1.8±0.87% and 4.8±2.9% using the square root and effective medium models, respectively. These errors were consistent with or smaller than the RD values shown in Table 2. The smaller error values obtained from the error propagation analysis compared with the RD values in Table 2 may be attributed to the mixing model which represents ideal conditions that may deviate from the actual arrangement of cuttings. Nevertheless, the error propagation analysis demonstrated that most of the variation of the estimated bulk

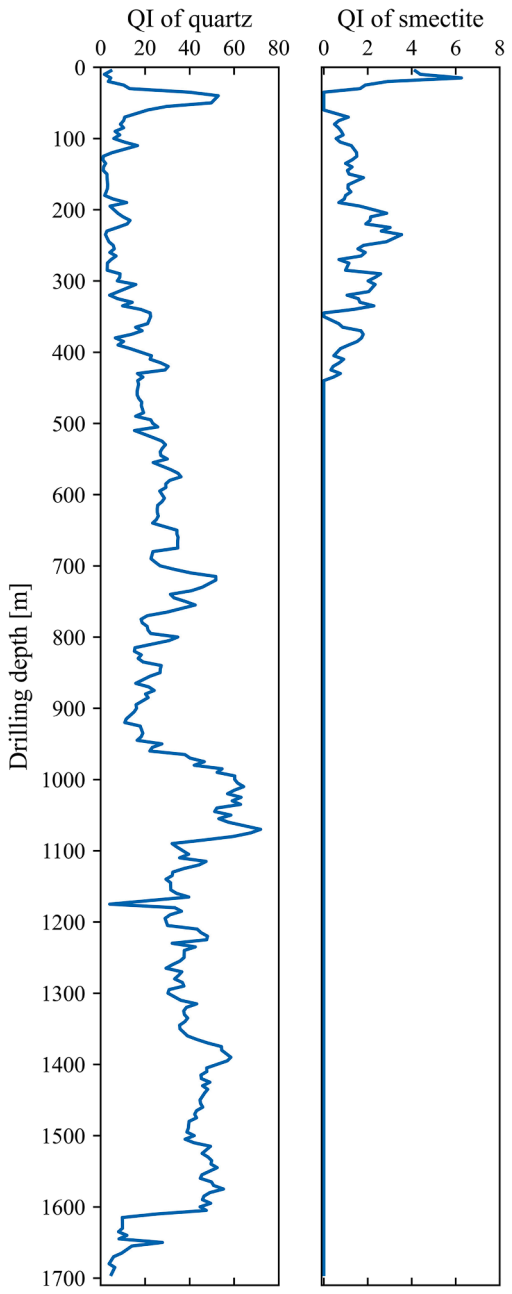

Fig. 13. Quartz index (QI) values of quartz and smectite along the target well (based on NEDO, 2007; 2009; Ojima et al., 2020).

TCs could be explained by these error sources.

In addition to the above error sources, anisotropy of rock mass may influence the accuracy of the bulk TC obtained from the drill cuttings. Previous studies have pointed out that TC anisotropy of rocks exists owing to internal structures of rocks such as laminations, mineral compositions and fracture orientations (Popov and Mandel, 1998; Davis et al., 2007). The TC anisotropies of rocks used in this study were not measured because the measurements assumed an isotropic medium. In addition, the use of cores obtained from a borehole did not allow shaping of cores in different directions. Considering that volcanic and pyroclastic rocks show isotropic TC compared with metamorphic rocks and shales (Davis et al., 2007), and the bulk TCs obtained from the cuttings in Section 3.1 were almost consistent with those of the cores, the influence of TC anisotropy on the measured rock cuttings in this study may be negligible. However, the magnitude of TC anisotropy has been shown to vary from rock to rock, even for the same species (Popov and Mandel, 1998); thus, rocks with substantial anisotropy may induce errors in the TC obtained from their drill cuttings.

6. Conclusions

This study proposed and examined a TC measurement method for drill cuttings using an original probe based on the transient plane source principle. To accurately obtain bulk and solid TCs from drill cuttings, the choice of mixing model is important. For the first time, this study quantitively compares the choices of five mixing models to determine TC from drill cuttings. The comparison showed that the suitable mixing models for TC estimation from drill cuttings of igneous and pyroclastic rocks were the square root and effective medium models, although the geometric model has previously been used for that purpose. In addition, the proposed method can measure and estimate practical bulk TC, as the errors between measured and estimated bulk TCs were within 10%, except for one granite sample. These results demonstrated the effectiveness of the transient plane source principle for quick and reliable TC measurement.

The measurement method was applied to drill cuttings obtained from a well in the Hachimantai geothermal field, Japan, and the solid and bulk TCs along the well were estimated. The estimated solid TCs aligned with the characteristic lithology of the well, and a linear regression analysis with mineral constituents confirmed that silica has a strong effect on the solid TC. Further, the analysis of the temperature profile using the TCs delineated the depth interval that could not be explained by thermal conduction, thereby identifying possible fluid-flow zones in the well. As such, the dense TC measurements from drill cuttings enables a detailed understanding at depths in geothermal fields.

The major limitation of TC determination from drill cuttings is the random variation of measurements, mainly owing to random packing of the drill cuttings. An effective way to reduce the random variation is by measuring samples multiple times. Further, the anisotropy of TC cannot be evaluated from the drill cuttings. Thus, for rock types with potentially large anisotropic TC, anisotropy may be better evaluated from available core samples. Despite these limitations, the dense measurement of TCs from drill cuttings by the proposed method is useful because of its cost-effectiveness, easy sample preparation and measurement accuracy. The measured TC can be applied in many aspects of geothermal development, such as characterizing geothermal reservoirs, determining the thermal properties for hydrothermal simulations, and identifying potential fluid-flow zones.

Funding

K.I. was partly funded by the Japan Society for the Promotion of Science (JSPS) KAKENHI (grant no. 20K15219).

CRediT authorship contribution statement

Haruto Sugamoto: Conceptualization, Methodology, Validation, Formal analysis, Investigation, Data curation, Software, Writing – original draft, Writing – review & editing, Visualization. **Kazuya Ishitsuka:** Conceptualization, Methodology, Resources, Investigation, Data curation, Software, Writing – original draft, Writing – review & editing, Supervision, Project administration, Funding acquisition. **Weiren Lin:** Conceptualization, Methodology, Resources, Data curation, Writing – original draft, Writing – review & editing, Supervision, Project administration. **Takemi Sakai:** Resources, Data curation, Writing – review & editing.

Declaration of Competing Interest

The authors declare that they have no known competing financial interests or personal relationships that could have appeared to influence the work reported in this paper.

Data availability

We have submitted the data as supplemental materials with this paper.

Acknowledgments

The authors acknowledge that the geothermal core samples stored at the National Institute of Advanced Industrial Science and Technology (AIST) were used for this study. The authors thank Shun Hashimoto for his assistance with the experiments and in constructing the calibration curve shown in Fig. 5.

Supplementary materials

Supplementary material associated with this article can be found, in the online version, at doi:10.1016/j.geothermics.2023.102742.

References

Adler, D., Flora, L.P., Senturia, S.D., 1973. Electrical conductivity in disordered systems. Solid State Commun. 12, 9–12. https://doi.org/10.1016/0038-1098(73)90333-5.

Akatsuka, T., Saito, R., Kajiwara, T., Osada, K., Nagaso, M., Watanabe, N., Asanuma, H., Kanetsuki, T., 2022. Geothermal geology and comprehensive temperature model based on surface and borehole geology in Sengan, northeast Japan. Geothermics 105, 102485. https://doi.org/10.1016/j.geothermics.2022.102485.

Alonso-Sánchez, T., Rey-Ronco, M.A., Carnero-Rodríguez, F.J., Castro-García, M.P., 2012. Determining ground thermal properties using logs and thermal drill cutting analysis. First relationship with thermal response test in principality of Asturias, Spain. Appl. Therm. Eng. 37, 226–234. https://doi.org/10.1016/j.applthermaleng.2011.11.020.

Beardsmore, G.R., Cull, J.P., 2001. Crustal Heat Flow: A Guide to Measurement and Modelling. Cambridge University Press, Cambridge.

Brigaud, F., Vasseur, G., Caillet, G., 1992. Thermal state in the north Viking Graben (North Sea) determined from oil exploration well data. Geophysics 57, 69–88. https://doi.org/10.1190/1.1443190.

Brigaud, F., Vasseur, G., Caillet, G., 1989. Use of well log data for predicting detailed in situ thermal conductivity profiles at well sites and estimation of lateral changes in main sedimentary units at basin scale. In: Proceedings of the ISRM International Symposium. ISRM-IS-1989-051.

Bruggeman, D.A.G., 1935. Berechnung verschiedener physikalischer Konstanten von heterogenen Substanzen. I. Dielektrizitätskonstanten und Leitfähigkeiten der Mischkörper aus isotropen Substanzen. Ann. Phys. 416, 636–664. https://doi.org/10.1002/andp.19354160705.

Bulmer, M.G., 1979. Principles of Statistics. Dover, New York, USA.

Chopra, N., Ray, L., Satyanarayanan, M., Elangovan, R., 2018. Evaluate best-mixing model for estimating thermal conductivity for granitoids from mineralogy: a case study for the granitoids of the Bundelkhand craton, central India. Geothermics 75, 1–14. https://doi.org/10.1016/j.geothermics.2018.03.011.

Clauser, C., 2009. Heat transport processes in the earth's crust. Surv. Geophys. 30, 163–191. https://doi.org/10.1007/s10712-009-9058-2.

Davis, M.G., Chapman, D.S., Wagoner, T.M.V., Armstrong, P.A., 2007. Thermal conductivity anisotropy of metasedimentary and igneous rocks. J. Geophys. Res. 112, B05216. https://doi.org/10.1029/2006JB004755.

Flóvenz, Ó.G., Saemundsson, K., 1993. Heat flow and geothermal processes in Iceland. Tectonophysics 225, 123–138. https://doi.org/10.1016/0040-1951(93)90253-G.

Fuchs, S., Balling, N., Förster, A., 2015. Calculation of thermal conductivity, thermal diffusivity and specific heat capacity of sedimentary rocks using petrophysical well logs. Geophys. J. Int. 203, 1977–2000. https://doi.org/10.1093/gji/ggv403.

Fuchs, S., Förster, H.J., Braune, K., Forster, A., 2018. Calculation of thermal conductivity of low-porous, sotropic plutonic rocks of the crust at ambient conditions from modal mineralogy and porosity: a viable alternative for direct measurement? J. Geophys. Res. Solid Earth 123, 8602–8614. https://doi.org/10.1029/2018JB016287.

Fuchs, S., Schutz, F., Förster, H.J., Förster, A., 2013. Evaluation of common mixing models for calculating bulk thermal conductivity of sedimentary rocks: correction charts and new conversion equations. Geothermics 47, 40–52. https://doi.org/10.1016/j.geothermics.2013.02.002.

Gustafsson, S.E., 1991. Transient plane source techniques for thermal conductivity and thermal diffusivity measurements of solid materials. Rev. Sci. Instrum. 62, 797–804. https://doi.org/10.1063/1.1142087.

Haffen, S., Geraud, Y., Diraison, M., Dezayes, C., 2013. Determination of fluid-flow zones in a geothermal sandstone reservoir using thermal conductivity and temperature logs. Geothermics 46, 32–41. https://doi.org/10.1016/j.geothermics.2012.11.001.

Hanai, T., 1968. Electrical properties of emulsions. In: Sherman, P. (Ed.), Emulsion Science. Academic Press, New York, pp. 354–477.

Harada, S., Tanaka, K., Inui, H., 2010. Thermoelectric properties and crystallographic shear structures in titanium oxides of the Magnèli phases. J. Appl. Phys. 108, 083703 https://doi.org/10.1063/1.3498801.

Hartmann, A., Pechnig, R., Clauser, C., 2008. Petrophysical analysis of regional-scale thermal properties for improved simulations of geothermal installations and basin-scale heat and fluid flow. Int. J. Earth Sci. 97, 421–433. https://doi.org/10.1007/s00531-007-0283-y.

Hayashi, M., 1979. Quantitative descriptions of cores and cuttings from geothermal wells. J. Geotherm. Res. Soc. Jpn. 1, 103–116. https://doi.org/10.11367/grsj1979.1.103 (in Japanese with English abstract).

He, Y., 2005. Rapid thermal conductivity measurement with a hot disk sensor Part 1. Theoretical considerations. Thermochim. Acta 436, 122–129. https://doi.org/10.1016/j.tca.2005.06.026.

International Organization for Standardization (ISO), 2008. ISO 22007-2:2008 plastics — determination of thermal conductivity and thermal diffusivity — part 2: transient plane heat source (hot disc) method. ISO, Geneva.

Ishitsuka, K., Ojima, H., Mogi, T., Kajiwara, T., Sugimoto, T., Asanuma, H., 2022. Characterization of hydrothermal alteration along geothermal wells using unsupervised machine-learning analysis of X-ray powder diffraction data. Earth Sci. Inform. 15, 73–87. https://doi.org/10.1007/s12145-021-00694-3.

Kämmlein, M., Stollhofen, H., 2019. Lithology-specific influence of particle size distribution and mineralogical composition on thermal conductivity measurements of rock fragments. Geothermics 80, 119–128. https://doi.org/10.1016/j.geothermics.2019.03.001.

Kimbara, K., 1985. An overview of the geothermal system in the Sengan geothermal area, northern Japan. J. Geotherm. Res. Soc. Jpn. 7 (3), 189–220. https://doi.org/10.11367/grsj1979.7.189 (in Japanese with English abstract).

Kiyohashi, H., Watanabe, T., Kyo, M., 1991. Continuous measurement of effective thermal conductivity of well cuttings - water mixture at geothermal conditions by hot-wire method under transient temperature field. Exp. Therm Fluid Sci. 4, 432–440. https://doi.org/10.1016/0894-1777(91)90006-D.

Kiyohashi, H., Watanabe, T., Kyo, M., Yoshimura, Y., Tanaka, S., 1989. Estimation of the effective thermal conductivity of rocks in situ by cuttings -part 2: heat conduction analysis of cuttings-water mixture beds and case studies for a test well at Fushime geothermal field, Kyushu, Japan-. J. Jpn. Assoc. Pet. Technol. 54, 474–483. https://doi.org/10.3720/japt.54.474 (in Japanese with English abstract).

Lee, T., Henyey, T.L., Damiata, B.N., 1986. A simple method for the absolute measurement of thermal conductivity of drill cuttings. Geophysics 51, 1580–1584. https://doi.org/10.1190/1.1442208.

Li, X., Cai, L., Liu, S., Li, X., 2020. Thermal properties of evaporitic rocks and their geothermal effects on the Kuqa foreland basin, Northwest China. Geothermics 88, 101898. https://doi.org/10.1016/j.geothermics.2020.101898.

Lichtenecker, K., 1924. Der elektrische Leitungswiderstand künstlicher und natürlicher Aggregate. Phys. Z. 25, 169–181, 193–204, 226–233.

Lin, W., Fulton, P.M., Harris, R.N., Tadai, O., Matsubayashi, O., Tanikawa, W., Kinoshita, M., 2014. Thermal conductivities, thermal diffusivities, and volumetric heat capacities of core samples obtained from the Japan Trench Fast Drilling Project (JFAST). Earth Planets Space 66, 48. https://doi.org/10.1186/1880-5981-66-48.

Lin, W., Hirose, T., Tadai, O., Tanikawa, W., Ishitsuka, K., Yang, X., 2020. Thermal conductivity profile in the Nankai accretionary prism at IODP NanTroSEIZE site C0002: estimations from high-pressure experiments using input site sediments. Geochem. Geophys. Geosyst. 21, e2020GC009108 https://doi.org/10.1029/2020GC009108.

Lin, W., Tadai, O., Hirose, T., Tanikawa, W., Takahashi, M., Mukoyoshi, H., Kinoshita, M., 2011. Thermal conductivities under high pressure in core samples from IODP NanTroSEIZE drilling site C0001. Geochem. Geophys. Geosyst. 12 https://doi.org/10.1029/2010GC003449.

Lippert, K., Ahrens, B., Nehler, M., Balcewicz, M., Mueller, M., Bracke, R., Immenhauser, A., 2022. Geothermal reservoir characterisation of devonian carbonates in north Rhine-Westphalia (W. Germany): mineralogy- and depofacies-related extrapolation of petrophysical parameters. Geothermics 106, 102549. https://doi.org/10.1016/j.geothermics.2022.102549.

Maldaner, C.H., Munn, J.D., Coleman, T.I., Molson, J.W., Parker, B.L., 2019. Groundwater flow quantification in fractured rock boreholes using active distributed temperature sensing under natural gradient conditions. Water Resour. Res. 55, 3285–3306. https://doi.org/10.1029/2018WR024319.

Mathis, N., 2000. Transient thermal conductivity measurements – comparison of destructive and non-destructive techniques. In: Proceedings of the 15th European Conference on Thermophysical Properties, p. P16.

Moeck, I.S., 2014. Catalog of geothermal play types based on geologic controls. Renew. Sustain. Energy Rev. 37, 867–882. https://doi.org/10.1016/j.rser014.05.032.

Morgan, P., 1975. Porosity determinations and the thermal conductivity of rock fragments with application to heat flow on Cyprus. Earth Planet. Sci. Lett. 26, 253–262. https://doi.org/10.1016/0012-821X(75)90093-X.

NEDO (New Energy and Industrial Technology Development Organization), 2009. Report on geothermal promotion survey at the Hachimantai area (3rd). New Energy and Industrial Technology Development Organization (NEDO). https://geothermal.jogmec.go.jp/report/nedo/file/25.pdf (in Japanese).

NEDO (New Energy and Industrial Technology Development Organization), 2007. Mid-term report on geothermal promotion survey at the Hachimantai area (2nd). New Energy and Industrial Technology Development Organization (NEDO). https://geothermal.jogmec.go.jp/report/nedo/file/25.pdf (in Japanese).

Ojima, H., Ishitsuka, K., Mogi, T., Tatsuya, K., Sugimoto, T., Asanuma, H., 2020. Extraction of features of strata using borehole data of geothermal area by multivariate analysis. In: Proceedings of the JpGU-AGU Joint Meeting 2020.

Popov, E., Trofimov, A., Goncharov, A., Abaimov, S., Chekhonin, E., Popov, Y., 2018. Technique of rock thermal conductivity evaluation on core cuttings and non-consolidated rocks. Int. J. Rock Mech. Min. Sci. 108, 15–22. https://doi.org/10.1016/j.ijrmms.2018.05.005.

Popov, Y.A., Pribnow, D.F.C., Sass, J.H., Williams, C.F., Burkhardt, H., 1999. Characterization of rock thermal conductivity by high-resolution optical scanning. Geothermics 28, 253–276. https://doi.org/10.1016/S0375-6505(99)00007-3.

Popov, Y., Mandel, A., 1998. Geothermal study of anisotropic rock masses. Izv Phys. Solid Earth 34 (11), 903–915.

Pribnow, D.F.C., Sass, J.H., 1995. Determination of thermal conductivity for deep boreholes. J. Geophys. Res. 100, 9981–9994. https://doi.org/10.1029/95JB00960. B6.

Ray, L., Forster, H.J., Forster, A., Fuchs, S., Naumann, R., Appelt, O., 2015. Tracking the thermal properties of lower continental crust: measured versus calculated thermal conductivity of high-grade metamorphic rocks (southern granulite province, India). Geothermics 55, 138–149. https://doi.org/10.1016/j.geothermics.2015.01.007.

Reuss, A., 1929. Berechnung der Fließgrenze von Mischkristallen auf Grund der Plastizitätsbedingung für Einkristalle. ZAMM - J. Appl. Math. Mech. 9, 49–58. https://doi.org/10.1002/zamm.19290090104. /Zeitschrift für Angewandte Mathematik und Mechanik.

Rey-Ronco, M.A., Alonso-Sánchez, T., Coppen-Rodríguez, J., Castro-García, M.P., 2013. A thermal model and experimental procedure for a point-source approach to determining the thermal properties of drill cuttings. J. Math. Chem. 51, 1139–1152. https://doi.org/10.1007/s10910-012-0097-4.

Robertson, E.C., Peck, D.L., 1974. Thermal conductivity of vesicular basalt from Hawaii. J. Geophys. Res. (1896-1977) 79, 4875–4888. https://doi.org/10.1029/JB079i032p04875.

Roy, R.F., Beck, A.E., Touloukian, Y.S., 1989. Thermophysical properties of rocks. In: Touloukian, Y.S., Judd, W.R., Roy, R.F. (Eds.), Physical Properties of Rocks and Minerals, CINDAS Data Series on Material Properties. Hemisphere Publishing Corporation, pp. 409–502.

Sanner, B., Hellstrom, G., Spitler, J., Gehlin, S., 2013. More than 15 years of mobile thermal response test – a summary of experiences and prospects. In: Proceedings of the European Geothermal Congress.

Sass, J.H., Lachenbruch, A.H., Munroe, R.J., 1971. Thermal conductivity of rocks from measurements on fragments and its application to heat-flow determinations. J. Geophys. Res. (1896-1977) 76, 3391–3401. https://doi.org/10.1029/JB076i014p03391.

Sen, P.N., Scala, C., Cohen, M.H., 1981. A self-similar model for sedimentary rocks with application to the dielectric constant of fused glass beads. Geophysics 46, 781–795. https://doi.org/10.1190/1.1441215.

Sharqawy, M.H., 2013. New correlations for seawater and pure water thermal conductivity at different temperatures and salinities. Desalination 313, 97–104. https://doi.org/10.1016/j.desal.2012.12.010.

Shibutani, S., Lin, W., Sado, K., Aizawa, A., Koike, K., 2022. An ancient >200m cumulative normal faulting displacement along the futagawa fault dextrally ruptured during the 2016 Kumamoto, Japan, Earthquake identified by a multiborehole drilling program. Geochem. Geophys. Geosyst. 23, e2021GC009966 https://doi.org/10.1029/2021GC009966.

Spitler, J.D., Gehlin, S.E.A., 2015. Thermal response testing for ground source heat pump systems – an historical review. Renew. Sustain. Energy Rev. 50, 1125–1137. https://doi.org/10.1016/j.ser.2015.05.061.

Takahashi, R., Matsueda, H., Okrugin, V.M., Ono, S., 2007. Epithermal gold-silver mineralization of the asachinskoe deposit in South Kamchatka, Russia. Resour. Geol. 57, 354–373. https://doi.org/10.1111/j.1751-3928.2007.00034.x.

The Geothermal Research Society of Japan (GRSJ), 2014. Geothermal Energy Handbook. Ohmsha Ltd, Tokyo (in Japanese).

Voigt, W., 1928. A determination of the elastic constants for beta-quartz lehrbuch de kristallphysik. Terubner Leipzig 40, 2856–2860.

Yi, F., Qi, X., Zheng, X., Yu, H., Bai, W., Bao, H., 2021. Method for determining the thermal conductivity of *in situ* formation rock using drilling cuttings. AIP Adv. 11, 065015 https://doi.org/10.1063/5.0051586.

Zhang, C., Guo, Z., Liu, Y., Cong, X., Peng, D., 2014. A review on thermal response test of ground-coupled heat pump systems. Renew. Sustain. Energy Rev. 40, 851–867. https://doi.org/10.1016/j.rser.2014.08.018.

Zhang, C., Jiang, G.Z., Shi, Y.Z., Wang, Z.T., Wang, Y., Li, S.T., Jia, X.F., Hu, S.B., 2018. Terrestrial heat flow and crustal thermal structure of the Gonghe-Guide area, northeastern Qinghai-Tibetan plateau. Geothermics 72, 182–192. https://doi.org/10.1016/j.geothermics.2017.11.011.